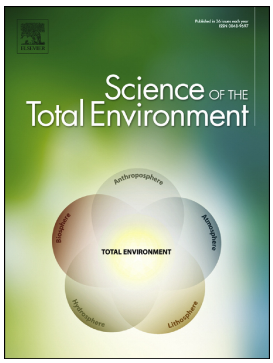

Relation between land cover and landslide susceptibility in Val d'Aran, Pyrenees (Spain): Historical aspects, present situation and forward prediction

Heping Shu, Marcel Hürlimann, Roberto Molowny-Horas, Marta González, Jordi Pinyol, Clàudia Abancó, Jinzhu Ma

PII: S0048-9697(19)33477-1
DOI: https://doi.org/10.1016/j.scitotenv.2019.07.363
Reference: STOTEN 33557

To appear in: *Science of the Total Environment*

Received date: 29 April 2019
Revised date: 26 June 2019
Accepted date: 22 July 2019

Please cite this article as: H. Shu, M. Hürlimann, R. Molowny-Horas, et al., Relation between land cover and landslide susceptibility in Val d'Aran, Pyrenees (Spain): Historical aspects, present situation and forward prediction, Science of the Total Environment, https://doi.org/10.1016/j.scitotenv.2019.07.363

Relation between land cover and landslide susceptibility in Val d'Aran, Pyrenees (Spain): historical aspects, present situation and forward prediction

Heping SHU[1,2*], Marcel HÜRLIMANN[1*], Roberto MOLOWNY-HORAS[3], Marta GONZÁLEZ[4], Jordi PINYOL[4], Clàudia ABANCÓ[1,4], Jinzhu MA[2],

1) *Division of Geotechnical Engineering and Geosciences, Department of Civil and Environmental Engineering, UPC BarcelonaTECH, Jordi Girona 1-3, 08034 Barcelona, Spain*
2) *Key Laboratory of Western China's Environmental Systems (Ministry of Education), College of Earth and Environmental Sciences, Lanzhou University, 222 South Tianshui Road, Lanzhou, 730000, China*
3) *CREAF, Campus Universitat Autonoma Barcelona, Edifici C, 08193 Bellaterra (Cerdanyola del Vallès), Catalonia, Spain*
4) *Department of Geotechnical and Geological Hazard Prevention, Cartographic and Geological Institute of Catalonia, Parc de Montjuïc S/N, 08038, Barcelona, Spain*

*Corresponding author: Heping SHU; Marcel HÜRLIMANN;
e-mail: shuhp15@lzu.edu.cn; marcel.hurlimann@upc.edu

Abstract

The effects of land use and land cover (LULC) dynamics on landslide susceptibility is not fully understood. This study evaluates the influence of LULC on landslide susceptibility and assesses the historic and future LULC changes in a high mountain region.

A detailed inventory map showing the distribution of landslides was prepared based on the 2013 episode in Val d'Aran, Pyrenees (Spain). This inventory showed that LULC clearly affected landslide susceptibility. Both the number of landslides and the landslide density triggered in grassland and meadow was highest (52% and 2.0 landslides/km^2). In contrast, the landslide density in areas covered by forest and shrubs was much lower (15% and 0.4 landslides/km^2, and 23% and 1.7 landslides/km^2, respectively).

Historical changes of LULC between 1946 and 2013 were determined by comparing aerial photographs. The results indicated that the forest and shrub areas increased by 68 and 65%, respectively; whereas grassland and scree areas decreased by 33 and 52%. Urban area also increased by 532%, especially between 1990 and 2001. Future LULC was predicted until 2097 using TerrSet software. The results showed that the forest area and urban area increased by 57 and 43%, severally; while shrubs, grassland and scree area decreased by 28, 46 and 78%, respectively.

Heuristic and deterministic models were applied to create susceptibility maps, which classified the study area into four susceptibility degrees from very low to high. The maps were validated by the 2013 landslide dataset and showed satisfactory results using receiver operating characteristics curves and density graph method. Then, susceptibility maps until 2097 were calculated by the heuristic model and results revealed that landslide susceptibility will decrease by 48% for high-susceptible areas.

In contrast, the areas of very-low susceptibility degree will increase 95%, while medium and low-susceptible areas will be more or less constant.

This study only includes the effect of future LULC changes on the landslide susceptibility and does not analyze the future impacts of climate changes and the variation of rainfall conditions. Nevertheless, the results may be used as support for land management guidelines to reduce the risk of slope instabilities.

Keywords: slopes; land use; cover type; landslide susceptibility; modelling; Pyrenees

1. Introduction

Landslides are important geomorphologic processes on most natural slopes, and contribute strongly to the sediment flux in mountainous terrain (Hovius et al. 1997). Herein, we mostly focus on rainfall-induced landslides including shallow slope failures and hillslope debris flows (Hungr et al. 2014). They constitute an essential hazard for both land degradation and infrastructure or buildings, sometimes even killing residents of the affected area.

Landslide susceptibility can be defined in various ways. A common definition is the probability of a slope failure based on the spatial distribution of previous slope failures and the effects of local terrain conditions on this distribution (Guzzetti et al. 2005; Fell et al. 2008). It reflects the degree to which a given terrain unit is likely to be affected by future slope movements (Guzzetti et al. 2006; Günther et al. 2013). Many research methods have been developed to evaluate landslide susceptibility at different scales, including statistical methods, heuristic approaches, mapping with a geographic information system, and physical models (Chen et al. 2016; Reichenbach et al. 2018).

Vegetation is widely accepted to stabilize slopes against landslides. Therefore, obtaining information about land use and land cover dynamics is outmost importance, and that dynamics must be taken into account to mitigate the hazard of slope mass-wasting. Hereafter, we will use land use and land cover (LULC) to describe both anthropogenic land uses and natural or semi-natural vegetation cover. Glade (2003) described a case study in New Zealand, where human action obviously changed the land use and adverse changes in land use played an important role in the occurrence of landslides. This and other studies (e.g. Goetz et al. 2015) support the idea that deforestation may play an important role in the propensity to earthfall episodes. In the

northern Italian Apennines, Persichillo et al. (2017) found that abandonment of cultivated land augmented the susceptibility to landslides. In addition, other researchers (Jakob 2000; Beguería 2006; Rickli and Graf 2009; Chen and Huang 2013) have analyzed the effects of natural vegetation recovery and found that the presence of vegetation decreased the occurrence of shallow landslides with forests having a particularly significant effect because of their deeper roots. Finally, to quantify the relationship between slope failures and forest cover, Schmaltz et al. (2017) used long-term landslide inventories to develop an empirical relationship with forest cover in Austria. All these investigations suggest that the vegetation cover creates an important stabilizing effect against landslides and that forested areas are less prone to slope failure than other vegetation types.

The effect of plant roots on slope stability has also been investigated from a geotechnical perspective (Cano et al. 2002; Genet et al. 2008; Mao et al. 2014; Liu et al. 2016). The Wu model (Wu et al., 1979) and the fiber-bundle model (Kun et al., 2006) were developed to quantify the reinforcement of slope stability by vegetation (Schwarz et al. 2010). Researchers have used physical models to demonstrate that land use changes at a regional scale affect the spatial and temporal probability of slope stability (Vanacker et al. 2003; Van Beek and Van Asch 2004; Reichenbach et al. 2014). Mugagga et al. (2012) analyzed deforestation and cultivation of steep slopes on Mount Elgon (Uganda) and confirmed the stabilizing effect of tree roots. These authors showed that slope stability strongly depends on LULC changes, but they did not attempt to predict the effects of future land use changes.

A number of methods have been developed to determine the dependence of future LULC changes on biotic drivers, such as species dispersion and plant diversity, and abiotic drivers, such as climate and topography. These methods generally apply

statistical methods (e.g. binomial regression) or machine learning (e.g. neural networks) to observational datasets that include a range of LULC categories (Stefanov et al. 2001; Aitkenhead and Aalders 2009; Ralha et al. 2013; Hyandye 2015; Ali Khawaldah 2016; Patil et al. 2017). The analyses often allow users to incorporate spatial information about protected areas, road networks, and other land use categories into the analysis (Jiang et al. 2015; Yirsaw et al. 2017; Chen et al. 2018). The resulting LULC models can then be employed to predict near-term and mid-term changes. That, in turn, helps landscape managers and researchers to guide their decisions based on simulated scenarios, and to evaluate the consequences of their decisions. The algorithms and decision rules behind these methods are available in a number of commercial and free software packages (Mas et al. 2014) .

The main goal of this study is to improve our understanding of the relationship between historic and future LULC changes and landslide susceptibility. Secondary objectives include: i) the analysis of the landslides triggered during the 2013 episode in the Val d'Aran (Pyrenees), and ii) the assessment of LULC evolution between 1946 and 2097. In addition, the results provide scientific support for future land-use planning and landslide prevention in a high mountain region affected by LULC changes. The paper is structured as follows: First, the 2013 landslide inventory was analyzed and the governing factors of the slope failures determined. Then, past change and predicted LULC were assessed. Finally, different models were applied to calculate the landslide susceptibility maps over a time span of 150 years (1946 – 2097)

2. Study area

2.1. Geologic, morphologic, and climatic settings

Our research was conducted in the Val d'Aran administrative region, which is located in the Spanish part of the Central Pyrenees (Fig. 1a). Its capital (Vielha) has a population of about 5000 inhabitants, whereas the region's total population is about 10000 inhabitants. The study area covers 336 km^2 and is a typical high mountain valley of glacial origin. The elevations range from about 1000 m asl at the valley floor (the location of Vielha) to almost 2750 m asl at the highest surrounding peaks. The Garonne River drains most of the region through France, where it flows into the Atlantic Ocean.

Figure 1

The study area is situated in the Axial zone of the Pyrenees. The Pyrenees started their uplift about 40 million years ago, and are constituted by materials from the Ordovician period to the Devonian period, with Tardi-Hercynian intrusions (Muñoz, 1992). The set of folds and thrusts is aligned from ESE to WNW, in a similar direction to the general orientation of the Pyrenees.

The bedrock mainly comprises Paleozoic rock, folded during the Hercinian orogeny, and intrusions of tardohercinian plutonic rocks. The exhumation of these materials by orogeny of the Pyrenees was followed by fluvial and glacial erosion. There are three main geological units in the study area (Fontboté, 1991): i) the basement of Palaeozoic bedrock, ii) the Mesozoic and Tertiary sediments, and iii) the

quaternary superficial formations, that mostly consist of colluvium and glacial deposits.

Glaciation has strongly affected the study area's present geomorphology, especially the last glaciations during the Upper Pleistocene (e.g., Bordonau 1992; Pallàs et al. 2006). During the last glacial maximum in the Pyrenees, ice covered much of the Val d'Aran, with a thickness estimated up to 1000 m. Other signs of glacial remodeling of the landscape include the U-shaped forms of some valleys and the presence of moraine sediments deposited by glaciers. As a consequence of the glacial dynamics and the posterior incision of the fluvial network, there are many steep slopes susceptible to landslides, snow avalanches and other mass-wasting processes.

The study area's climate is dominated by two factors: the prevailing west winds from the Atlantic Ocean, and the orographic effects of the Pyrenees. The average annual precipitation ranges from about 900 mm in the valley floor to 1200 mm on the highest peaks. The mean annual temperature is between 5 and 9 °C in the study area, (CAC, 2004). Precipitation that has historically triggered landslides is associated with two main rainfall patterns: prolonged rainfall episodes in the autumn or spring, and convective rainstorms in summer. In winter, precipitation is mostly snowfall, which can contribute to landslide triggering conditions when melting.

Several episodes of high landslide activity have affected the study area along the 20th century. The most relevant ones are also associated to flood events: October 1907, August 1963, and September/November 1982 (Hürlimann et al. 2003; Victoriano et al. 2016).

2.2. Land use and land cover

The present LULC in the study area is shown in Figure 2a by the orthophotograph of 2013, which is published by the Cartographic and Geological Institute of Catalonia (ICGC, http://www.icc.cat/vissir3). The official inventory (Land Cover Map of Catalonia) published by the Ecological and Forestry Applications Research Center (CREAF, http://www.creaf.cat/) was used to assess and quantify LULC in the study area. The original Land Cover Map of 2013 was reclassified into five general LULC categories: i) forest, ii) shrubs, iii) grassland and meadow, iv) scree, and v) others (Fig. 2b). The reclassified LULC map was compared with the slope orientation and a strong relation was detected, especially for forest category (Fig. 2c). In contrast to the two categories shrubs and grassland and meadow, which are more abundant on south-facing slopes, the forest category is more common on north-facing slopes. These results are supported by other studies that revealed a strong influence of solar radiation on differences in ecosystem communities and soil development (Veblen and Donnegan, 2005; Birkeland et al. 2003; McGuire et al. 2016). Finally, the area of scree is relatively uniformly distributed in all slope aspects.

Figure 2

3. The 2013 landslide episode

3.1. Causes and landslide types

An important landslide event occurred in the Central Pyrenees after a heavy rainfall episode in the 17th and the 18th of June 2013. This event also caused exceptional flooding of the Garonne and Noguera Pallaresa river valleys (Oller et al.

2013), and the total economic losses were estimated to more than 100 million euros (Victoriano et al. 2016).

The flooding and landsliding events were caused by the combination of two exceptional factors: i) extreme rainfall (124.7 mm in 48 h, of which 101.2 mm fell on the 18th June) and ii) high meltwater volumes after an unusually heavy snowfall during the winter (Fig. 3). The meteorological station at Bonaigua (2266 m asl) (IGC, 2013) recorded the largest snowfall since observation started in 1997. Even in early June 2013, a snowpack of more than 300 cm was measured at the station. As a consequence, on the 18th of June a peak discharge of 300 m^3/s was estimated at the Garonne river at Bossost village (CHE, 2013), which represents the highest value in the catchment area since 1937 (Pineda et al. 2013).

Figure 3

A landslide inventory was created based on different data available: a) photographs taken during emergency helicopter flights just after the event and b) sets of aerial photographs taken by the ICGC on 22nd of June and 21st to 23rd of July 2013. All these photographs have a resolution of 25 cm per pixel and they were compared with aerial photographs taken during 2012. Finally, we performed field surveys to validate the inventory.

The slope failures observed in the 2013 episode can be divided into three types considering the updated Varnes classification (Hungr et al. 2014): i) small and shallow planar slides, which mostly involved uppermost soil layer (Fig. 4a), ii) large slope failures (translational as well as rotational slides), which include thicker soil layers and sometimes also weathered bedrock (Fig. 4b); and iii) debris avalanches

(also called hill-slope debris flows), which formed a narrow path down the slope until the debris spread out at the bottom of the slope (Fig. 4c, 4d; Pinyol et al. 2017).

Figure 4

3.2. Analysis of the landslide inventory

High-quality landslide inventories are important to calibrate and validate models of landslide susceptibility and to evaluate the performance of physical slope stability models (Brardinoni and Church 2004; van den Eeckhaut et al. 2010; Petschko et al. 2016). The resulting inventory for the Val d'Aran 2013 episode consists of 393 events within the study area (Fig. 5). All data were integrated into Quantum GIS (https://qgis.org, v.2.18.25) together with attributes such as geomorphological characteristics or landslide type.

Figure 5

A 2-m resolution DEM was used to analyze the relationship between the geomorphological governing factors and landslide occurrence. The slope angle, aspect degree and curvature were extracted from the DEM by applying the terrain analysis tools of QGIS software. In addition, the elevation was determined by conducting the identify feature tools. After a preliminary analysis, four of them were selected as governing factors due to their relevance on the slope failure analysis: elevation, slope angle, orientation (aspect degree), and plan curvature. We divided the geomorphological governing factors into different intervals based on their current situation and the number of landslides was calculated for each interval. Finally, the

landslide density was computed by dividing the number of landslides by the total landslide area in each interval (Fig. 6).

Figure 6

Landslides were mainly distributed between 1600 m and 2200 m asl, with the greatest frequency between 2000 m and 2100 m (Fig. 6a). The landslide density was highest for elevations ranging between 1700 and 2100 m, especially in the range from 1700 and 1800 m as well as from 2000 and 2100 m.

For the slope angle, landslides mainly occurred at slope angles between 25° and 45°, which accounted for 81% of the total landslides (Fig. 6b). The landslide density gradually increased with higher slopes and reaches the maximum at 35° ~ 40°.

Regarding the aspect degree, landslides were mainly initiated on south-facing slopes with the maximum on southwest-facing slopes (Fig. 6c). In contrast, there were relatively few landslides distributed on north-facing slopes. This difference of landslide density at opposite slopes can be associated with the corresponding land use and land cover and was commented in the previous section and in other studies (e.g. McGuire et al. 2016).

In terms of curvature, the number of landslides was greatest for negative or near-zero curvature (Fig. 6d). The density decreased continuously with curvature increasing from negative (convex) to positive (concave). This suggests that landslides were concentrated in concave slopes. It could be explained by the fact that concave areas retain moisture better than convex areas and as a result, an increase on soil moisture content could bring the material to critical condition to trigger a landslide.

Regarding geological factors like lithology or the distance to a fault, the inventory revealed an insignificant influence of these factors on the landslide initiation. In contrast, there was a strong relation between LULC and slope failures. The most important LULC categories affected by the 2013 episode were forest, shrubs, grassland and meadow, and scree (Fig. 7). The number of landslides was highest for grassland and meadow, which accounted for 52% of the total number. Shrubs and forest represented 15 and 23%, respectively, and scree corresponds to the remaining 10%. Since the proportions of the total area were greatest for grassland and forest, at 32 and 43%, the landslide density was highest for the grassland. These results illustrated that the LULC strongly affected the spatial distribution of landslides.

Figure 7

4. Methods

4.1. Analysis of LULC changes

4.1.1. Historical evolution

Online available aerial orthophotographs of the study area from 1946, 1956, 1990, 2001, and 2013 were analyzed (http://www.icc.cat/vissir3). While images before 1990 were available only in black-and-white, subsequent images were in color. The different LULC-categories were visually delineated from each year's images, by applying standard methods to detect and quantify differences in color, object, area, and other attributes (Singh 1989; Persichillo et al. 2017). We specially used the color information of the orthophotographs for the differentiation between the LULC categories only focusing on areas larger than 0.2 km^2. Four periods of land use

changes between the five available images were defined. The final categories were divided into forest, shrubs, grassland and meadow, urban areas, and scree. Urban land was excluded from our analysis because we detected no landslides originated in urban areas. In order to confirm our visual interpretations and to determine the accuracy of our visual interpretation, the data of the official pan-European inventory CORINE (https://land.copernicus.eu/pan-european/corine-land-cover, version 1990) were used.

4.1.2. LULC prediction

The results of the historical analysis were used to perform a predictive analysis of future changes on LULC. The classified images from the period 1990-2013, in raster format, were used as inputs of the Land Change Modeler (LCM) software, which is part of the IDRISI TerrSet software suite (Eastman 2015). A key step in such analysis is the selection of the predictor variables, on which the observed changes may depend. For the present study, we chose a set of predictor variables that previous work (Molowny-Horas et al. 2015) had shown to be substantial drivers of land use change (Table 1).

Table 1

Selected predictor variables were divided into three categories:

a) Climatic. We used the following climatic variables in raster format (original pixel size: 200 m × 200 m) calculated by Ninyerola et al (2005): total annual precipitation, mean annual temperature, mean minimum and maximum temperatures and mean annual solar radiation.
b) Topographic: We used the European Digital Elevation Model (EU-DEM v1.1, https://land.copernicus.eu/) as the elevation model for the study area (original

pixel size: 25 m × 25 m). We used the EU-DEM instead of the aforementioned 2x2m DEM because the original pixel size of the former was much closer to the pixel size in the LULC maps. Aspect and slope were calculated using the "terrain" function of the "raster" R package (Hijmans 2017). The curvature was computed by implementing the method proposed by Evans (1980) in the R software (R project website https://www.r-project.org/).

c) Landscape: closest distance to rivers, roads and urban centres were calculated from the 2001 LULC maps with the function "distance" of the raster R package (Hijmans 2017). Assuming that the expansion of urban area and, especially, of road infrastructures in this alpine area takes place at a low rate, relative to changes in other land covers, we assumed these three variables could be kept constant throughout the calculations.

All variables were projected using a common reference system, and were resampled to an identical pixel size (30 m × 30 m) and cropped to have the same spatial extent in the study area.

4.2. Susceptibility models applied

Heuristic and deterministic models were applied to calculate the landslide susceptibility. For both cases, results were reclassified into four different susceptibility classes (very low, low, medium, high).

4.2.1. Heuristic method (HM)

The advantage of heuristic methods are the simplicity and easy application (Fell et al. 2008). Herein, a two-parameter method is used including slope angle and LULC. As already detected in many other studies, the slope angle is also in this study one of

the most important governing factors to define landslide susceptibility (Fig. 6). In addition, there is an important effect of the land use and land cover type (Fig. 7).

A simple susceptibility matrix was defined based on the combinations of LULC and slope angle (Fig. 8). LULC categories include forest, shrub, grassland and meadow (called "grass" in the matrix), scree, and other (urban area or water bodies), while the slope angle classes are: <10°, 10 to 20°, 20 to 30°, and >30°. The matrix evaluates each pixel in the study area and assigns to it one of four possible susceptibility classes.

Figure 8

4.2.2. Deterministic model: infinite-slope method (DM)

To quantify the slope stability, a deterministic infinite-slope stability model was adopted. We used a simple model proposed by Vanacker et al. (2003), which calculates the slope stability based on the conventional limit-equilibrium method, represented as a factor of safety (*FS*). The FS represents the ratio of the available shear strength (τ_f) to the shear stress (τ). According to the Mohr-Coulomb failure criterion (Bromhead 1992), the available shear strength of a slope can be defined as:

$$\tau_f = c' + \Delta_c + (\sigma - \mu)\tan\phi' \qquad (1)$$

where c' represents the soil cohesion, Δc represents the root cohesion, σ represents the total normal stress, μ represents the pore water pressure, and ϕ' represents the angle of soil internal friction (Selby 1993). The shear stress can be expressed as:

$$\tau = \gamma_t z \sin\alpha \cos\alpha \qquad (2)$$

where γ_t represents the total unit weight of the sliding material (kN/m^3), z represents the depth of the failure plane (m), and α is the slope angle (°).

By combining equations 1 and 2, *FS* can be represented as:

$$FS = \frac{c' + \Delta_c + (\gamma_t - \gamma_w m) z \cos^2 \alpha}{\cos^2 \alpha \, \gamma_t z \, sin \, \alpha \, \cos \alpha} \tan \phi' \qquad (3)$$

where γ_w represents the unit weight of water, and *m* represents the normalized height of the water table above the failure surface. These parameters were obtained from the research literature (Vanacker et al. 2003; Bathurst et al. 2006; Hürlimann et al. 2010; GITS-UPC 2010; Liu et al. 2011; Bregoli et al. 2015), and the specific values for each LULC categories are shown in Table 2. There are uncertainties in the values, but we selected average values that are common in such regional stability calculations. The values are based on experimental results, field observations as well as expert criteria.

Table 2

4.2.3. Validation of the landslide susceptibility models

To validate the results of the heuristic and deterministic methods and to choose the optimal methodology, the density method (this method has been described in the section 3.2) and the receiver operating characteristic (ROC) curve were used (Beguería 2006; Vakhshoori and Zare 2016).

In the density method, the number of landslides, the area of each susceptibility class, and the landslide density were compared for the two susceptibility methods. The values of landslide density should increase from very low to high classes with an increasing susceptibility (Pradhan and Lee, 2010).

The ROC method consists in obtaining success curves of each of the susceptibility classes. The ROC curve compares the "true positive rate" with the "false positive rate" (Fawcett, 2006). The advantage of the ROC method is that it produces a threshold-independent curve (Fawcett 2006; Vakhshoori and Zare 2016).

5. Results and discussion

5.1. Analysis of LULC changes

5.1.1. Historical evolution

The analysis of the historical evolution on LULC changes based on the orthophotograph for selected ortho-images showed important changes in the study period between 1946 and 2013 (Fig. 9). A qualitative comparison gives an idea that the forest and urban area experienced important changes between 1946 and 2013, but especially between 1956 and 1990.

Figure 9

Figure 10 shows the observed LULC changes from 1946 to 2013 in a quantitative way, and also includes the predicted values until 2097. The total forest area increased constantly during the study period (Fig. 10a) by 68%. The area of shrubs also increased by 65%. The water bodies increased especially from 1956 to 1990 because of the construction of water reservoir. The urban area increased steadily until 1990, then the change accelerated. From 1946 to 2013 the total urban area increased by 532%. In contrast, the grassland and meadow area and the scree area decreased gradually from 1946 to 2013.

All these trends are supported by previous studies carried out in the Pyrenees and other nearby mountainous areas: the population decrease and agriculture land abandonment that occurred during the 20th century, after reaching a population peak in the 18th century, resulted in the development of shrub and forest ecosystems (Garcia-Ruiz and Lasanta-Martinez 1990; MacDonald et al. 2000; Mottet et al. 2006;

Beguería 2006). In addition, the increasing temperature may have facilitated the expansion of forest and shrub into higher elevation (Fisichelli et al. 2014; Kerns et al. 2018; Mckelvey and Buotte 2018)

Figure 10

To validate the results of the orthophotograph interpretation, we compared our 1990 cartography with the official 1990 CORINE survey results (https://land.copernicus.eu/pan-european/corine-land-cover). The comparison showed that there are only small differences in most of the LULC categories (Fig. 11). The CORINE areas of forest and scree were slightly larger (by 2.8 and 1.1 km^2, respectively) than the present results. In contrast, the CORINE areas of shrubs, grassland and meadow, urban area, and water bodies were smaller than the present results (by 4.0, 0.4, 0.3, and 0.2 km^2, respectively). The largest of these differences (for shrubs) represents <1.2% of the 336-km^2 study area, and the other dissimilarities were even smaller (0.1 to 0.8%), suggesting that our delineation of the historic LULC was acceptably accurate.

Figure 11

The earliest orthophotographs were black and white images, so it was difficult to distinguish some of the land uses during the visual interpretation process. Especially at the borders between land uses such as forest and shrubs, the colors of images and visual texture were similar, making them difficult to distinguish visually. Apart from these errors in the visual interpretation, the differences between the two

datasets may also be due to the fact that, because of its low resolution of 100 m × 100 m, the CORINE survey failed to include small natural bodies of water and scattered urban areas. In addition, the water reservoirs were not identified in the official inventory. Therefore, the water bodies and urban areas in the CORINE survey were less than those we calculated from the orthophotographs.

5.1.2. Future prediction

The future LULC situation was predicted from 2025 to 2097 based on IDRISI TerrSet simulation model (Fig. 10b). The total forest area continued to increase steadily throughout the simulation period. The forest area increased by 57% from 2013 to 2097, although that increment slowed over time. The shrub area decreased by 28%, showing its accelerated decrease towards the end of the prediction period. The area corresponding to the water bodies category remained unchanged. The predicted urban area continued to increase, and the rate of increase was 43%; but the growth gradually decreased after 2025, and especially after 2049. Both the grassland and meadow area, as well as the scree area, decreased steadily between 2013 and 2097 at a rate of 46% and 78%, respectively. The magnitude of the predicted decrease in grassland and meadow area was larger than the observed historical change. The decrease of the scree area matched the change in grassland and meadow area, and its rate of decline was greater than the historical rate, except for the more rapid decrease from 2001 to 2013.

5.2. Implications of LULC changes on landslide susceptibility zonation

5.2.1. Validation of the landslide susceptibility models

First, a qualitative validation using “landslide density” value for each susceptibility class was carried out (Fig. 12a). The landslide density rises for higher

susceptibility for both simulation methods. The rate of increase was larger for the deterministic method than for the heuristic method and the landslide density at high susceptibility class was at maximum for the deterministic method. However, the trend of the HM density curve is visually better than the one of DM (see low and very low susceptibility class).

Figure 12b shows the validation results for landslide susceptibility using the ROC analysis for the heuristic and deterministic methods. In the heuristic method, the AUC was 0.72, versus 0.75 for the deterministic method. These results suggest that there was little difference between the two methods in their ability to predict landslide susceptibility. Given that, since the heuristic method is much easier to apply and faster to calculate the susceptibility map, the results of heuristic method were used as a final result for landslide susceptibility.

Figure 12

5.2.2. Future changes in landslide susceptibility maps

The heuristic method (based on susceptibility matrix described in Figure 8) was used to produce maps of future landslide susceptibility. These maps incorporate temporal evolution of LULC, while slope angle is assumed to be constant over time. Fig. 13 compares the maps obtained using HM from historic (1946), present (2013) and future (2025 and 2097) LULC conditions. In general, the susceptibility maps confirm well-known aspects like that the relatively low elevation had very low susceptibility, whereas areas of low, medium and high susceptibility were mainly distributed on the slopes at high elevations, especially for the predicted future high-susceptibility (Fig. 13c, d).

Figure 14 shows the areas of different susceptibility classes calculated for all the resulting maps. The percentage of the area with low susceptibility was gradually increasing between 1946 and 2013, but its proportion remained roughly constant (27%) after 2025. The area of very low and medium class was always enlarged, whereas the area with high susceptibility was reduced. This may be because the scree area, grassland and meadow area have rapidly decreased by 89% and 64% since 1946, while the forest area has been increasing by 163% from 1946 to 2097. Beguería (2006) found that old forests can strongly increase slope stability, but young forests need a long time to produce effective slope protection. In addition, due to the low slope and high forest cover in the southeastern corner of the study area, the proportion of very low susceptibility was greatly augmented between 1946 and 2097. These results suggest that the study area will become increasingly stable in the future.

Figure 13

Figure 14.

The LULC changes in our study area predict a decrease of landslides occurrence, which agrees with previous researches on this topic (Blijenberg 1998; Glade 2003; Beguería 2006; Imaizumi et al., 2010; Persichillo et al. 2017)). A large area of land with low vegetation cover or shallow-rooted vegetation will evolve into grassland or forest (Reichenbach et al. 2014; Persichillo et al. 2017).

Here, only spatial probability of landsliding is investigated, thus rainfall under future climate changes are not considered. Moreover, previous research suggests that there have been no significant changes in either total rainfall or frequency of extreme

rainfall in our study area during the 20th century (García-Ruiz et al. 2001). The June 2013 episode is classified as exceptional, especially because it combined heavy rainfall and important snowmelt (Victoriano et al. 2016). Beniston (2003) presented mountains areas as "sentinels of climate changes" because the respond more promptly and effectively than other geographical environments to climate changes. Moreover, climate models showed that global warming will increase the frequency and intensity of severe rainfall events in the future, and it may produce more shallow slope failures (Gariano and Guzzetti 2016; Alvioli et al. 2018). Therefore, it is in regions like the one we have analyzed in the present study where the impact brought about by global warming will be easier to notice.

6. Conclusions

The effects of land use and land cover (LULC) dynamics on landslide susceptibility is of great importance not only for research purpose, but also for practical applications. We examined the interactions between land use change and landslide susceptibility over a time span of 150 years (from 1946 to 2097) in Val d'Aran, Pyrenees (Spain).

The analysis of the slope failures triggered in the 2013 episode highlighted that LULC has an important effect on the spatial occurrence of landslides. Both the number of landslides and the landslide density triggered in grassland and meadow was highest (52% and 2.0 landslides/km^2). In contrast, the landslide density in areas covered by forest and shrubs was much lower. The proportion of the number of landslides were 15 and 27 % in the forest and shrubs, and the densities were 0.4 landslides/km^2 and 1.7 landslides/km^2, respectively.

Historical changes of LULC were determined in a first task by the digitalization of the most important vegetation categories from aerial photographs of 1946, 1956,

1990, 2001 and 2013. The results revealed on one side that the areas of grassland and scree decreased by 33 and 52%, respectively. On the other side, the LULC evolution showed an important increase of forest (+68%) and shrubs area (+65%). Urban area increased by 532%, especially between 1990 and 2001. The future LULC was predicted until 2097 using TerrSet software. The results showed that the forested area and the urban area will increase by 57 and 43%, while the shrubs, grassland and scree will decrease by 28, 46 and 78%, respectively.

The heuristic and deterministic methods were applied to calculate the landslide susceptibility, which was divided into four landslide susceptibility classes (very low, low, medium and high). Moreover, the landslide susceptibility zonation obtained from heuristic method was first successfully validated with the 2013 landslide dataset by applying the receiver operating characteristics curves and the density graph method. Then, this method was applied to delineate the historic and future susceptibility maps using the observed and predicted LULC changes between 1946 and 2097. The results show that the high-susceptible areas of the map that was calculated for the predicted LULC of 2097, will decrease by 48%. In contrast, the areas of medium- and very-low susceptibility will increase by 7 and 95%, respectively, and the area of low susceptibility will be constant.

This study shows that the overall susceptibility conditions may improve in the future. However, it does not incorporate the future impacts of climate change and the variation of rainfall conditions. Such changes in the triggering rainfalls certainly affect future landslide occurrence and will be subject of forthcoming investigations. Nevertheless, the results of this study help to better understand the general trend of landslide susceptibility in the future and provide information for an adequate land management in order to better mitigate the risk of slope instabilities.

Acknowledgements:

The research was supported by the national research project "Slope mass-wasting under climate change (SMUCPHY)" funded by Spain's Ministry of Economy and Competitiveness (project reference number BIA 2015-67500-R) and co-funded by AEI/FEDER, UE. Heping Shu is grateful for financial support from the Chinese Scholarship Council during his studies at the Polytechnic University of Catalonia.

References

Aitkenhead, M.J., Aalders, I.H., 2009. Predicting land cover using GIS, Bayesian and evolutionary algorithm methods. J. Environ. Manage. 90, 236–250. https://doi.org/10.1016/j.jenvman.2007.09.010

Ali Khawaldah, H., 2016. A Prediction of Future Land Use/Land Cover in Amman Area Using GIS-Based Markov Model and Remote Sensing. J. Geogr. Inf. Syst. 8, 412–427. https://doi.org/10.4236/jgis.2016.83035

Alvioli, M., Melillo, M., Guzzetti, F., Rossi, M., Palazzi, E., von Hardenberg, J., Brunetti, M.T., Peruccacci, S., 2018. Implications of climate change on landslide hazard in Central Italy. Sci. Total Environ. 630, 1528–1543. https://doi.org/10.1016/j.scitotenv.2018.02.315

Bathurst, J.C., Burton, A., Clarke, B.G., Gallart, F., 2006. Application of the SHETRAN basin-scale, landslide sediment yield model to the Llobregat basin, Spanish Pyrenees. Hydrol. Process. 20, 3119–3138

Beguería, S., 2006. Changes in land cover and shallow landslide activity: A case study in the Spanish Pyrenees. Geomorphology. 74, 196–206. https://doi.org/10.1016/j.geomorph.2005.07.018

Beniston, M., 2003. Climatic Change in Mountain Regions : 5–31

Birkeland, P., R. Shroba, S. Burns, A. Price, and P. Tonkin., 2003. Integrating soils and geomorphology in mountains—an example from the Front Range of Colorado, Geomorphology, 55(1), 329–344

Blijenberg, H., 1998. Rolling stones? Triggering and frequency of hillslope debris flows in the Bachelard Valley, southern French Alps. Ned. Geogr. Stud

Bordonau, J., 1992. Els complexos glàcio-lacustres relacionats amb el darrer cicle glacial als Pirineus. Geoforma Ediciones, Logroño

Brardinoni, F., Church, M., 2004. Representing the landslide magnitude–frequency relation: Capilano River basin, British Columbia. Earth Surf. Process. Landforms 29, 115–124. https://doi.org/10.1002/esp.1029

Bregoli, F., Medina, V., Chevalier, G., Hürlimann, M., Bateman, A., 2015. Debris-flow susceptibility assessment at regional scale: Validation on an alpine environment. Landslides 12, 437–454. https://doi.org/10.1007/s10346-014-0493-x

Bromhead, E.N., 1992. The stability of slopes. Blackie academic & professional, London

CAC, 2004. Atles Climàtic Digital de Catalonia. [Climatic Atlas of Catalonia.] http://www.opengis.uab.cat/acdc/Last accessed 22 May 2015

Cano, A., Navia, R., Amezaga, I., Montalvo, J., 2002. Local topoclimate effect on short-term cutslope reclamation success. Ecol. Eng. 18, 489–498. https://doi.org/10.1016/S0925-8574(02)00010-1

CHE, 2013. Informe de la avenida del 17 al 20 de junio de 2013 en la cuenca del río Garona [Report of the avenue from June 17th to 20th, 2013 in the Garona river basin]. Confederación Hidrográfica del Ebro. Ministry for the Ecological Transition, Spain

Chen, C.Y., Huang, W.L., 2013. Land use change and landslide characteristics analysis for community-based disaster mitigation. Environ. Monit. Assess. 185, 4125–4139. https://doi.org/10.1007/s10661-012-2855-y

Chen, L.P., Sun, Y.J., Sajjad, S., 2018. Monitoring and predicting land use and land cover changes using remote sensing and GIS techniques—a case study of a hilly area, Jiangle, China. PLoS One 13:1–23. doi: 10.1371/journal.pone.0200493

Chen, L.X., van Westen, C.J., Hussin, H., Ciurean, R.L., Turkington, T., Chavarro-Rincon, D., Shrestha, D.P., 2016. Integrating expert opinion with modelling for quantitative multi-hazard risk assessment in the Eastern Italian Alps. Geomorphology 273, 150–167. https://doi.org/10.1016/j.geomorph.2016.07.041

Evans, I. S., 1980. An integrated system of terrain analysis and slope mapping. Zeitschrift fur Geomorphologie 36: 274-295

Eastman, J.R., 2015. TerrSet: Geospatial Monitoring and Modeling Software. Clark Labs 53, 392. https://doi.org/10.1017/CBO9781107415324.004

Fawcett, T., 2006. An introduction to ROC analysis. Pattern Recognit. Lett. 27, 861–874

Fell, R., Corominas, J., Bonnard, C., Cascini, L., Leroi, E., Savage, W.Z., 2008. Guidelines for landslide susceptibility, hazard and risk zoning for land-use planning. Eng. Geol. 102, 99–111. https://doi.org/10.1016/j.enggeo.2008.03.014

Fisichelli, N.A., Frelich, L.E., Reich, P.B., 2014. Temperate tree expansion into adjacent boreal forest patches facilitated by warmer temperatures. Ecography (Cop.). 37, 152–161. https://doi.org/10.1111/j.1600-0587.2013.00197.x

Fontboté, J, 1991. Reflexions sobre la tectònica dels Pirineus. Memorias la Real Acad. Ciencias y Artes Barcelona Tercera ép, 307–352

Garcia-Ruiz, J.M., Lasanta-Martinez, T., 1990. Land-Use Changes in the Spanish Pyrenees. Mt. Res. Dev. 10, 267. https://doi.org/10.2307/3673606

García-Ruiz, J.M., Beguería, S., López-Moreno, J.I., Lorente, A., Seeger, M., 2001. Los Recursos Hídricos Superficiales del Pirineo Aragone´s y Su Evolucio´n Reciente. Geoforma ediciones, Logroño

Gariano, S.L., Guzzetti, F., 2016. Landslides in a changing climate. Earth-Science Rev. 162, 227–252. https://doi.org/10.1016/j.earscirev.2016.08.011

Genet, M., Kokutse, N., Stokes, A., Fourcaud, T., Cai, X., Ji, J., Mickovski, S., 2008. Root reinforcement in plantations of Cryptomeria japonica D. Don: effect of tree age and stand structure on slope stability. For. Ecol. Manage. 256, 1517–1526. https://doi.org/10.1016/j.foreco.2008.05.050

GITS-UPC., 2010. Deliverable 2.1 - Methodologies to identify areas of high potential FF & DF risk. Technical report, IMPRINTS

Glade, T., 2003. Landslide occurrence as a response to land use change: a review of evidence from New Zealand. CATENA 51, 297–314. https://doi.org/https://doi.org/10.1016/S0341-8162(02)00170-4

Goetz, J.N., Guthrie, R.H., Brenning, A., 2015. Forest harvesting is associated with increased landslide activity during an extreme rainstorm on Vancouver Island, Canada. Nat. Hazards Earth Syst. Sci. 15, 1311–1330. https://doi.org/10.5194/nhess-15-1311-2015

Günther, A., Reichenbach, P., Malet, J.P., van Den Eeckhaut, M., Hervás, J., Dashwood, C., Guzzetti, F., 2013. Tier-based approaches for landslide susceptibility assessment in Europe. Landslides 10, 529–546. https://doi.org/10.1007/s10346-012-0349-1

Guzzetti, F., Reichenbach, P., Ardizzone, F., Cardinali, M., Galli, M., 2006. Estimating the quality of landslide susceptibility models. Geomorphology 81, 166–184. https://doi.org/10.1016/j.geomorph.2006.04.007

Guzzetti, F., Reichenbach, P., Cardinali, M., Galli, M., Ardizzone, F., 2005. Probabilistic landslide hazard assessment at the basin scale. Geomorphology 72, 272–299

Hijmans, R.J., 2017. raster: Geographic Data Analysis and Modeling. R package version 2.6-7. https://CRAN.R-project.org/package=raster

Hovius, N., Stark, C., Allen, P., 1997. Sediment flux from a mountain belt derived by landslide mapping. Geology 25, 231–234

Hungr, O., Leroueil, S., Picarelli, L., 2014. The Varnes classification of landslide types, an update. Landslides 11, 167–194. https://doi.org/10.1007/s10346-013-0436-y

Hürlimann, M., Corominas, J., Moya, J., Copons, R., 2003. Debris-flow events in the Eastern Pyrenees. Preliminary study on initiation and propagation., in: Rickenmann, D., Chen, C. (Eds.), 3rd Int. Conf. on Debris-Flow Hazards Mitigation. Millpress, Davos, pp. 115–126

Hürlimann, M., Abancó, C., Moya, J., 2010. Debris-flow initiation affected by snowmelt. Case study from the Senet monitoring site, Eastern Pyrenees. Proceedings of the "Mountain Risks: Bringing science to society" International Conference. Firenze, Italy, pp.81-86

Hyandye, C., 2015. GIS and Logit Regression Model Applications in Land Use/Land Cover Change and Distribution in Usangu Catchment. Am. J. Remote Sens. 3, 6. https://doi.org/10.11648/j.ajrs.20150301.12

Imaizumi, F., Sidle, R.C., Kamei, R., 2010. Effects of forest harvesting on the occurrence of landslides and debris flows in steep terrain of central Japan. Earth Surf. Process. Landforms 33, 827–840

IGC., 2013. Gruixos de neu per temporades [Snow thicknesses per seasons] http://www.igc.cat/web/ca/allaus_gruix_neu_v2.php?t=1213&e=totes . ICGC, Cartographic and Geological Institute of Catalonia. Last accessed 18 June 2018.

Jakob, M., 2000. The impacts of logging on landslide activity at Clayoquot Sound, British Columbia. Catena 38, 279–300. https://doi.org/10.1016/S0341-8162(99)00078-8

Jiang, W., Chen, Z., Lei, X., Jia, K., Wu, Y., 2015. Simulating urban land use change by incorporating an autologistic regression model into a CLUE-S model. J. Geogr. Sci. 25, 836–850. https://doi.org/10.1007/s11442-015-1205-8

Kerns, B.K., Powell, D.C., Mellmann-Brown, S., Carnwath, G., Kim, J.B., 2018. Effects of projected climate change on vegetation in the Blue Mountains ecoregion, USA. Clim. Serv. 10, 33–43. https://doi.org/10.1016/j.cliser.2017.07.002

Kun, F., Raischel, F., Hidalgo, R.C., Herrmann, H.J., 2006. Extensions of fibre bundle models. Lect. Notes Phys. 705, 57–92. https://doi.org/10.1007/3-540-35375-5_3

Liu, G., Craig, J.R., Soulis, E.D., 2011. Applicability of the Green-Ampt Infiltration Model with Shallow Boundary Conditions. J. Hydrol. Eng. 16, 266–273. https://doi.org/10.1061/(ASCE)HE.1943-5584.0000308

Liu, H.W., Feng, S., Ng, C.W.W., 2016. Analytical analysis of hydraulic effect of vegetation on shallow slope stability with different root architectures. Comput. Geotech. 80, 115–120. https://doi.org/10.1016/j.compgeo.2016.06.006

MacDonald, D., Crabtree, J.R., Wiesinger, G., Dax, T., Stamou, N., Fleury, P., Gutierrez Lazpita, J., Gibon, A., 2000. Agricultural abandonment in mountain areas of Europe: Environmental consequences and policy response. J. Environ. Manage. 59, 47–69. https://doi.org/10.1006/jema.1999.0335

Mao, Z., Yang, M., Bourrier, F., Fourcaud, T., 2014. Evaluation of root reinforcement models using numerical modelling approaches. Plant Soil 381, 249–270. https://doi.org/10.1007/s11104-014-2116-7

Mas, J.F., Kolb, M., Paegelow, M., Camacho Olmedo, M.T., Houet, T., 2014. Inductive pattern-based land use/cover change models: A comparison of four

software packages. Environ. Model. Softw. 51, 94–111. https://doi.org/10.1016/j.envsoft.2013.09.010

McGuire, L. A., Rengers, F. K., Kean, J. W., Coe, J. A., Mirus, B. B., Baum, R. L., & Godt, J. W. (2016). Elucidating the role of vegetation in the initiation of rainfall-induced shallow landslides: Insights from an extreme rainfall event in the Colorado Front Range. Geophysical Research Letters, 43(17), 9084–9092. https: doi:10.1002/2016gl070741

Mckelvey, K.S., Buotte, P.C., 2018. Climate Change and Rocky Mountain Ecosystems. https://doi.org/10.1007/978-3-319-56928-4

Molowny-Horas, R., Basnou, C., Pino, J., 2015. A multivariate fractional regression approach to modeling land use and cover dynamics in a Mediterranean landscape. Comput. Environ. Urban Syst. 54, 47–55. https://doi.org/10.1016/j.compenvurbsys.2015.06.001

Mottet, A., Ladet, S., Coqué, N., Gibon, A., 2006. Agricultural land-use change and its drivers in mountain landscapes: A case study in the Pyrenees. Agric. Ecosyst. Environ. 114, 296–310. https://doi.org/10.1016/j.agee.2005.11.017

Mugagga, F., Kakembo, V., Buyinza, M., 2012. Land use changes on the slopes of Mount Elgon and the implications for the occurrence of landslides. Catena 90, 39–46. https://doi.org/10.1016/j.catena.2011.11.004

Muñoz, A., 1992. Evolution of a continental collision belt: ECORS-Pyrenees crustal balanced cross-section, in: McClay, K.R. (Ed.), Thrust Tectonics. Chapman & Hall, pp. 235–246

Ninyerola, M., Pons, X., Roure, J.M., 2005. Atlas Climático Digital de la Península Ibérica. Metodología y aplicaciones en bioclimatología y geobotánica. ISBN 932860-8-7. Universidad Autónoma de Barcelona, Bellaterra

Oller, P., Pinyol, J., González, M., Ripoll, J., Micheo, J., 2013. Efectes Geomorfològics De L ' Aiguat I Riuada Del 18 De Juny De 2013 209–211

Pallàs, R., Rodés, A., Braucher, R., Carcaillet, J., Ortuño, M., Bordonau, J., Bourlès, D., Vilaplana, J.M., Masana, E., Santanach, P., 2006. Late Pleistocene and Holocene glaciation in the Pyrenees: a critical review and new evidence from 10Be exposure ages, south-central Pyrenees. Quat. Sci. Rev. 25, 2937–2963

Patil, S.D., Gu, Y., Dias, F.S.A., Stieglitz, M., Turk, G., 2017. Predicting the spectral information of future land cover using machine learning. Int. J. Remote Sens. 38, 5592–5607. https://doi.org/10.1080/01431161.2017.1343512

Persichillo, M.G., Bordoni, M., Meisina, C., 2017. The role of land use changes in the distribution of shallow landslides. Sci. Total Environ. 574, 924–937. https://doi.org/https://doi.org/10.1016/j.scitotenv.2016.09.125

Petschko, H., Bell, R., Glade, T., 2016. Effectiveness of visually analyzing LiDAR DTM derivatives for earth and debris slide inventory mapping for statistical susceptibility modeling. Landslides 13, 857–872. https://doi.org/10.1007/s10346-015-0622-1

Pineda, N., Prohom, M., Serra, A., Martí, G., Garcia, C., Velasco, E., Gracia, A., 2013. Efectes geomorfològics de l'aiguat i riuada del 18 de juny de 2013. Proceedings of the conferences La gestió de les inundacions, November 27 and 28, 2013

Pinyol, J., González, M., Moysset, M., 2017. "Preliminary estimation of Aubeta debris flow deposition and erosion volumes using LIDAR data". JTC1 Workshop on Advances in Landslide Understanding. May 24 – 26, 2017, Barcelona, España

Pradhan, B., Lee, S., 2010. Delineation of landslide hazard areas on Penang Island, Malaysia, by using frequency ratio, logistic regression, and artificial neural

network models. Environ. Earth Sci. 60, 1037–1054. https://doi.org/10.1007/s12665-009-0245-8

Ralha, C.G., Abreu, C.G., Coelho, C.G.C., Zaghetto, A., Macchiavello, B., Machado, R.B., 2013. A multi-agent model system for land-use change simulation. Environ. Model. Softw. 42, 30–46. https://doi.org/10.1016/j.envsoft.2012.12.003

Reichenbach, P., Busca, C., Mondini, A.C., Rossi, M., 2014. The Influence of Land Use Change on Landslide Susceptibility Zonation: The Briga Catchment Test Site (Messina, Italy). Environ. Manage. 54, 1372–1384. https://doi.org/10.1007/s00267-014-0357-0

Reichenbach, P., Rossi, M., Malamud, B.D., Mihir, M., Guzzetti, F., 2018. A review of statistically-based landslide susceptibility models. Earth-Science Rev. 180, 60–91. https://doi.org/10.1016/j.earscirev.2018.03.001

Rickli, C., Graf, F., 2009. Effects of forests on shallow landslides-Case studies in Switzerland. For. Snow Landsc. Res. 82, 33–44.

Schmaltz, E.M., Steger, S., Glade, T., 2017. The influence of forest cover on landslide occurrence explored with spatio-temporal information. Geomorphology 290, 250–264. https://doi.org/10.1016/j.geomorph.2017.04.024

Schwarz, M., Preti, F., Giadrossich, F., Lehmann, P., Or, D., 2010. Quantifying the role of vegetation in slope stability: a case study in Tuscany (Italy). Ecol Eng 36, 285–291. https://doi.org/10.1016/j.ecoleng.2009.06.014

Selby, M.G., 1993. Hillslope Materials and Processes. Oxford Univ. Press, New York

Singh, A., 1989. Review Article Digital change detection techniques using remotely-sensed data, International Journal of Remote Sensing, 10:6, 989-1003. doi: 10.1080/01431168908903939

Stefanov, W.L., Ramsey, M.S., Christensen, P.R., 2001. Monitoring urban land cover change: An expert system approach to land cover classification of semiarid to arid urban centers. Remote Sens. Environ. 77, 173–185. https://doi.org/10.1016/S0034-4257(01)00204-8

Vakhshoori, V., Zare, M., 2016. Landslide susceptibility mapping by comparing weight of evidence, fuzzy logic, and frequency ratio methods. Geomatics, Nat. Hazards Risk 7, 1731–1752. https://doi.org/10.1080/19475705.2016.1144655

Van Beek, L.P.H., Van Asch, T.W.J., 2004. Regional assessment of the effects of land-use change on landslide hazard by means of physically based modelling. Nat. Hazards 31, 289–304. https://doi.org/10.1023/B:NHAZ.0000020267.39691.39

Vanacker, V., Vanderschaeghe, M., Govers, G., Willems, E., Poesen, J., Deckers, J., Bievre, B. De, 2003. Linking hydrological, infinite slope stability and land-use change models through GIS for assessing the impact of deforestation on slope stability in high Andean watersheds. Geomorphology 52, 299–315. https://doi.org/https://doi.org/10.1016/S0169-555X(02)00263-5

van den Eeckhaut, M., Marre, A., Poesen, J., 2010. Comparison of two landslide susceptibility assessments in the Champagne-Ardenne region (France). Geomorphology 115:141–155. doi: 10.1016/j.geomorph.2009.09.042

Veblen, T. T., and J. A. Donnegan., 2005. Historical range of variability for forest vege- tation of the national forests of the Colorado Front Range, USDA Forest Service, Rocky Mountain Region

Victoriano, A., García-Silvestre, M., Furdada, G., Bordonau, J., 2016. Long-term entrenchment and consequences for present flood hazard in the Garona River

(Val d'Aran, Central Pyrenees, Spain). Nat. Hazards Earth Syst. Sci. 16, 2055–2070. https://doi.org/10.5194/nhess-16-2055-2016

Wu, T.H., McKinnell III, W.P., Swanston, D.N., 1979. Strength of tree roots and landslides on Prince of Wales Island, Alaska. Can. Geotech. J. 16, 19–33. https://doi.org/10.1139/t79-003

Yirsaw, E., Wu, W., Shi, X., Temesgen, H., Bekele, B., 2017. Land Use/Land Cover change modeling and the prediction of subsequent changes in ecosystem service values in a coastal area of China, the Su-Xi-Chang region. Sustain. 9, 1–17. https://doi.org/10.3390/su9071204

Figures List:

Figure 9. Historical evolution of land use and land cover in the study area. Comparison of orthophotographs from (a) 1946, (b) 1990, (c) 2001, and (d) 2013.

Figure 10. Historic and future changes in LULC in the study area: a) observed changes between 1946 and 2013 based on visual interpretation of historical orthophotographs; b) predicted changes between 2025 and 2097 based on the IDRISI TerrSet software. Note that the y-axis scales greatly differ in the plots.

Figure 11. Validation of the historica land use and land cover changes by comparing of our cartography with the official CORINE inventory of 1990.

Figure 12. Comparison and validation of the susceptibility maps obtained by heuristic (HM) and deterministic (DM) approaches. a) Comparison of the number of landslides, and density between the two models for the four susceptibility classes. b) Results of the receiver operating characteristics analysis comparing the performance of the two susceptibility approaches.

Figure 13. Landslide susceptibility maps (heuristic method) showing the consequences of LULC changes. Historical susceptibility in (a) 1946 and (b) present conditions. Predicted future susceptibility in (c) 2049 and (d) 2097.

Figure 14. Evolution of susceptibility over time. Percentage of each susceptibility class between 1946 and 2097 in the study area.

Table 1. Predictor variables (calculated as explained in the text) used for the predictive model of LULC changes. Ranges of values for the variables are given for the study area. Mean values for climatic variables correspond to annual averages. Variable types are coded as C (climatic), T (topographic), and L (landscape).

Variable name	Type	Units	Range (min, max)
Mean temperature	C	ºC ×10	21, 92
Mean minimum temp.	C	ºC ×10	-40, 36
Mean maximum temp.	C	ºC ×10	77, 148
Total precipitation	C	mm ×10	6898, 12520
Radiation	C	kJ/ (m^2 day μm) ×10	1306, 2345
Elevation	T	m	906, 2464
Slope	T	Radians	0.08, 0.79
Curvature	T	Arbitrary	-0.005, 0.005
Aspect	T	Radians	0.11, 6.18
Distance to rivers	L	m	11, 1001
Distance to roads	L	m	42, 6825
Distance to urban	L	m	0, 3167

Table 2 Reclassification of LULC and assignation of parameters

Parameters LULC	c' (k*Pa*)	Δc (k*Pa*)	z (m)	ϕ' (°)	m (%)	γ_t (kg/m^3)	γ_w (kg/m^3)
Forest	0[a]	5[b, c]	3[b]	20[b, d]	50[b, d]	2000[b]	1000
Shrubs	0[a]	1[b]	2[b]	23[b, d]	50[b, d]	2000[b]	1000
Grassland	0[a]	0.5[b]	1[b]	23[b, d]	50[b, d]	2000[b]	1000
Scree	0[a]	0[a]	1[b]	40[b, d]	50[b, d]	2000[b]	1000
Urban area	0[a]	50[b]	0.1[b]	40[b, d]	50[b, d]	2000[b]	1000
Water bodies	ND	ND	ND	ND	ND	ND	ND

[a] Vanacker et al. (2003); [b] Bregoli et al. (2015); [c] Bathurst et al. (2006); [d] GITS-UPC (2010); ND: no data

Highlights:

• An inventory of about 393 landslides were created for the 2013 Val d'Aran episode.

• The analysis of the inventory showed a clear influence of LULC on the landslide susceptibility.

• Past observed and future predicted LULC changes were assessed.

• Landslide susceptibility maps were calculated over a time span of 150 years (1946 – 2097).

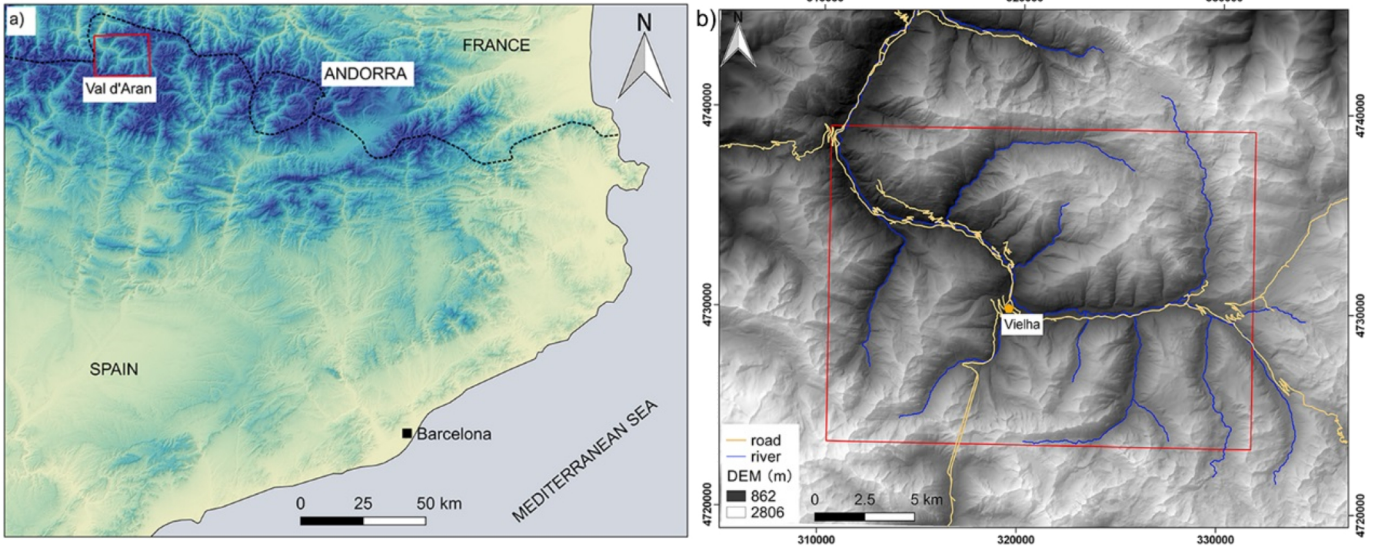
a)
FRANCE
ANDORRA
Val d'Aran
SPAIN
Barcelona
MEDITERRANEAN SEA
0 25 50 km
N
b)
310000
320000
330000
4740000
4730000
4720000
Vielha
road
river
DEM (m)
862
2806
0 2.5 5 km

Figure 1

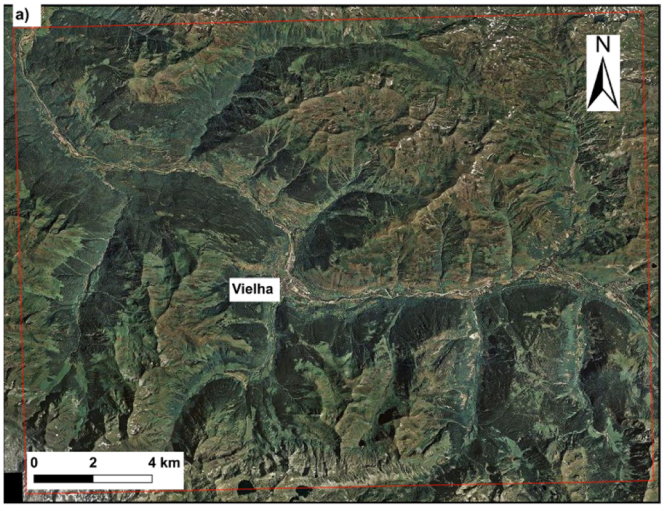
a)
N
Vielha
0 2 4 km

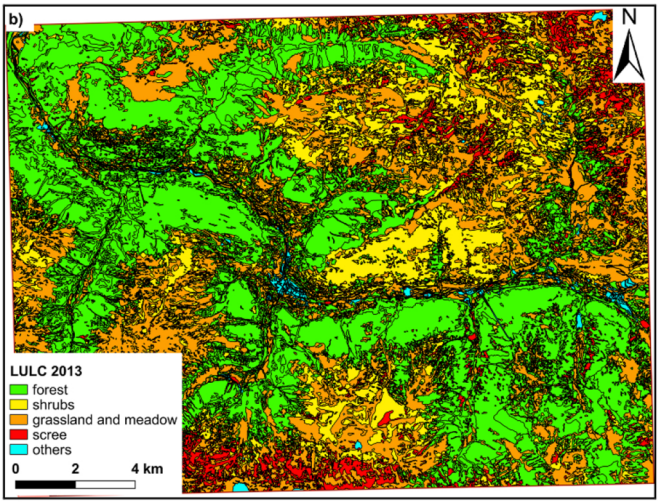
b)
N
LULC 2013
forest
shrubs
grassland and meadow
scree
others
0 2 4 km

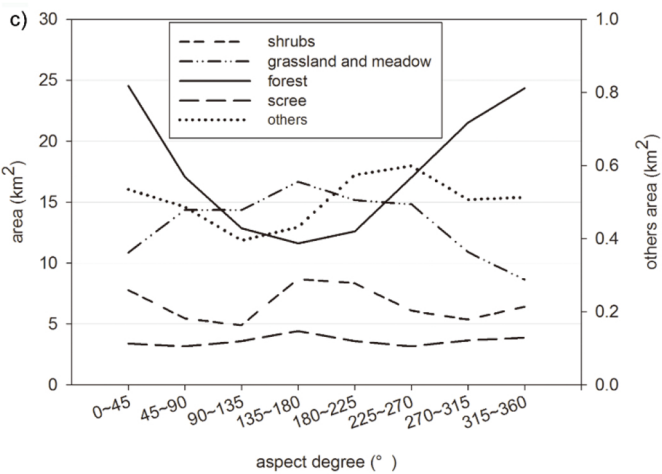
c)
shrubs
grassland and meadow
forest
scree
others
area (km2)
others area (km2)
0~45
45~90
90~135
135~180
180~225
225~270
270~315
315~360
aspect degree (°)

Figure 2

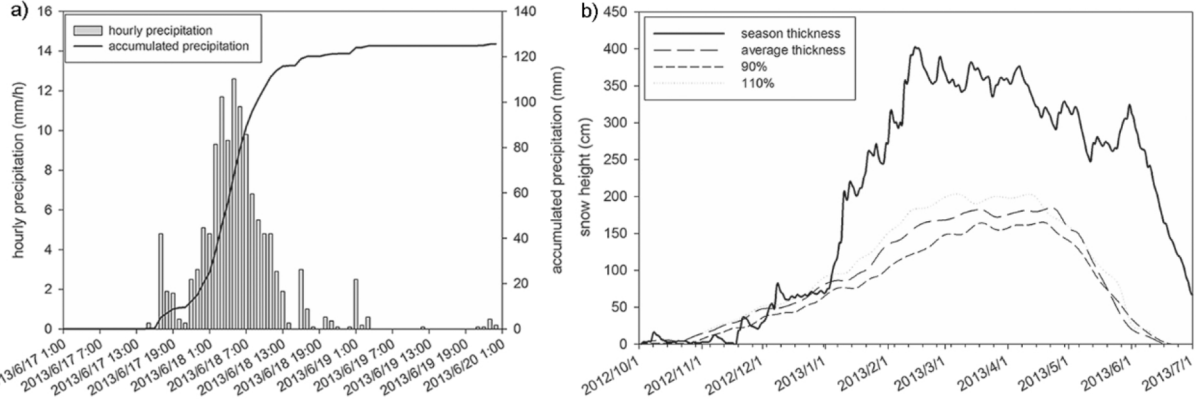
a)
hourly precipitation
accumulated precipitation
hourly precipitation (mm/h)
accumulated precipitation (mm)
0
2
4
6
8
10
12
14
16
0
20
40
60
80
100
120
140
2013/6/17 1:00
2013/6/17 7:00
2013/6/17 13:00
2013/6/17 19:00
2013/6/18 1:00
2013/6/18 7:00
2013/6/18 13:00
2013/6/18 19:00
2013/6/19 1:00
2013/6/19 7:00
2013/6/19 13:00
2013/6/19 19:00
2013/6/20 1:00
b)
season thickness
average thickness
90%
110%
snow height (cm)
0
50
100
150
200
250
300
350
400
450
2012/10/1
2012/11/1
2012/12/1
2013/1/1
2013/2/1
2013/3/1
2013/4/1
2013/5/1
2013/6/1
2013/7/1

Figure 3

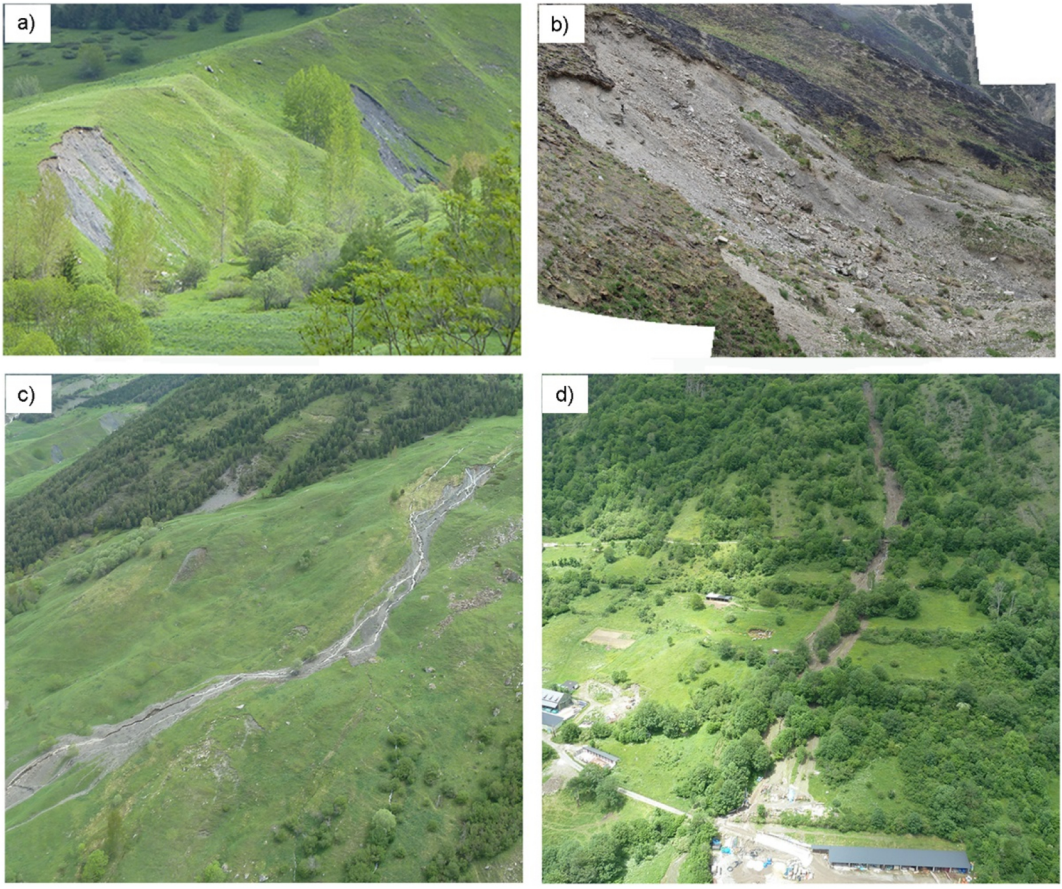

Figure 4

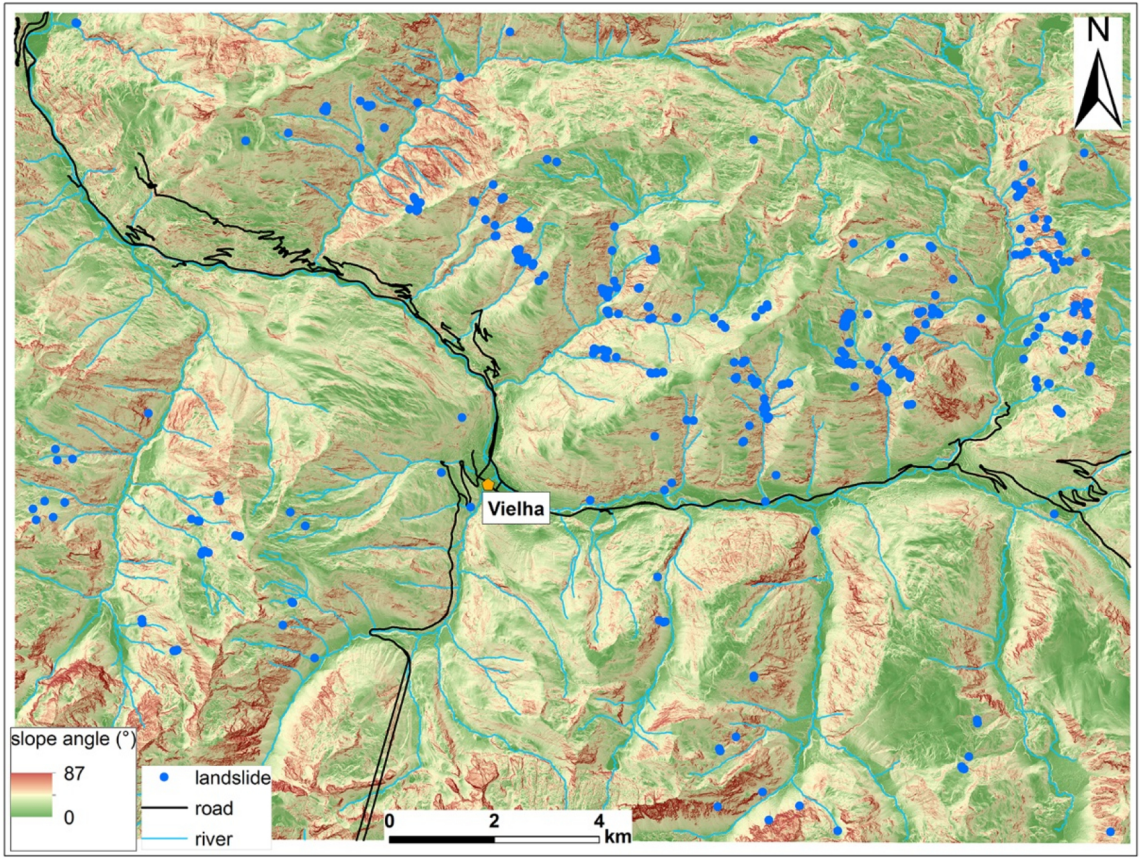

Figure 5

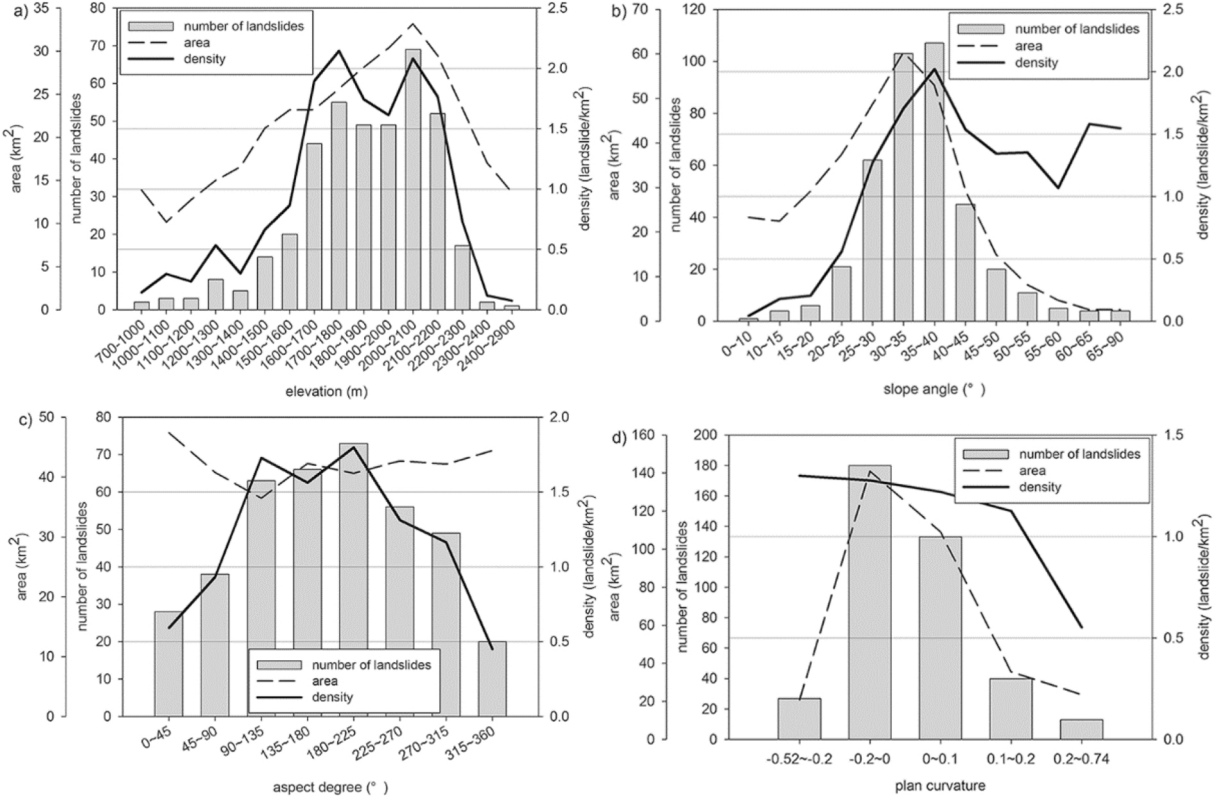
a)
number of landslides
area
density
area (km2)
number of landslides
density (landslide/km2)
700-1000
1000~1100
1100~1200
1200~1300
1300~1400
1400~1500
1500~1600
1600~1700
1700~1800
1800~1900
1900~2000
2000~2100
2100~2200
2200~2300
2300~2400
2400~2900
elevation (m)
b)
number of landslides
area
density
area (km2)
number of landslides
density (landslide/km2)
0~10
10~15
15~20
20~25
25~30
30~35
35~40
40~45
45~50
50~55
55~60
60~65
65~90
slope angle (°)
c)
number of landslides
area
density
area (km2)
number of landslides
density (landslide/km2)
0~45
45~90
90~135
135~180
180~225
225~270
270~315
315~360
aspect degree (°)
d)
number of landslides
area
density
number of landslides
area (km2)
density (landslide/km2)
-0.52~-0.2
-0.2~0
0~0.1
0.1~0.2
0.2~0.74
plan curvature

Figure 6

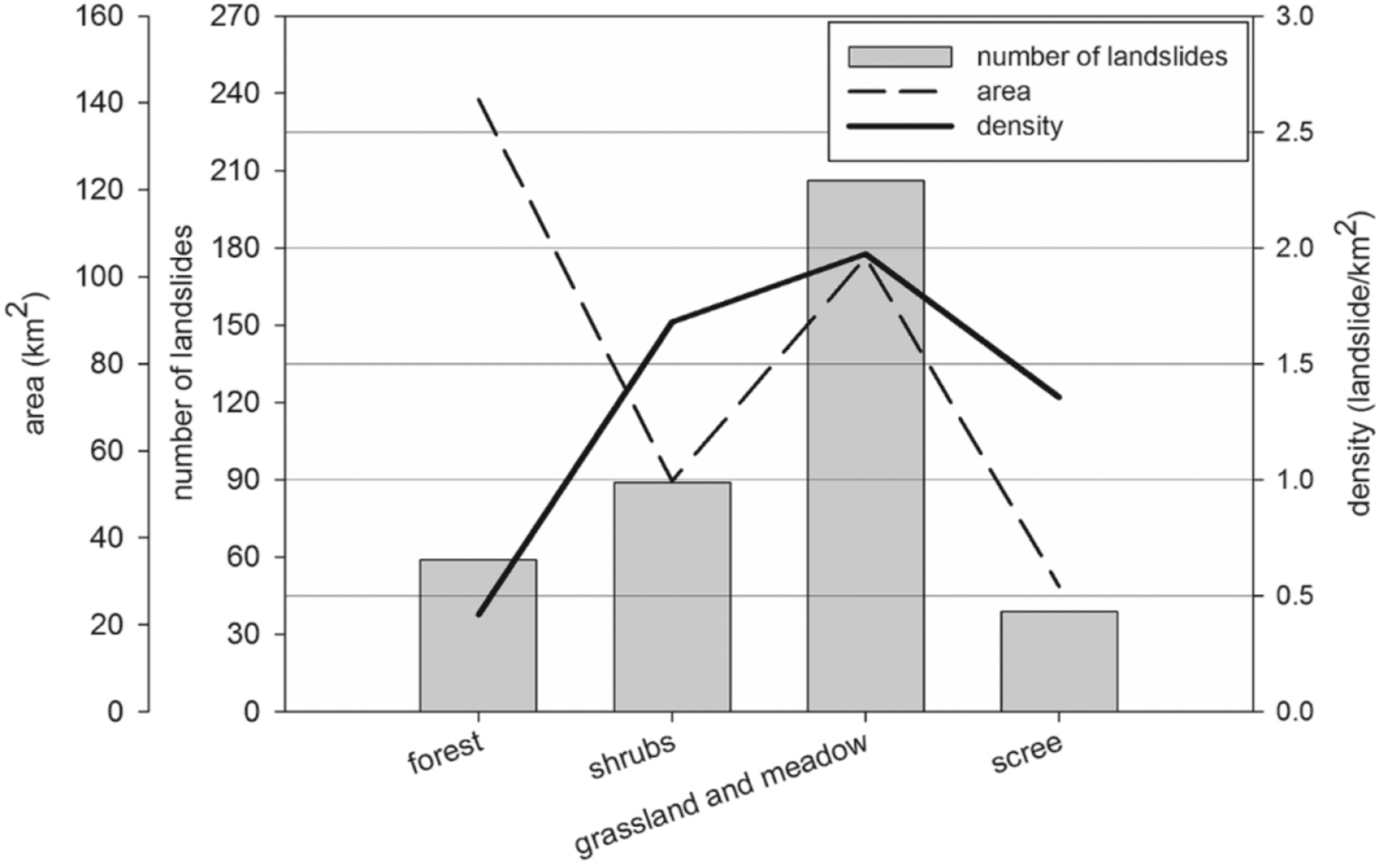
number of landslides
area
density
area (km2)
number of landslides
density (landslide/km2)
0
20
40
60
80
100
120
140
160
0
30
60
90
120
150
180
210
240
270
0.0
0.5
1.0
1.5
2.0
2.5
3.0
forest
shrubs
grassland and meadow
scree

Figure 7

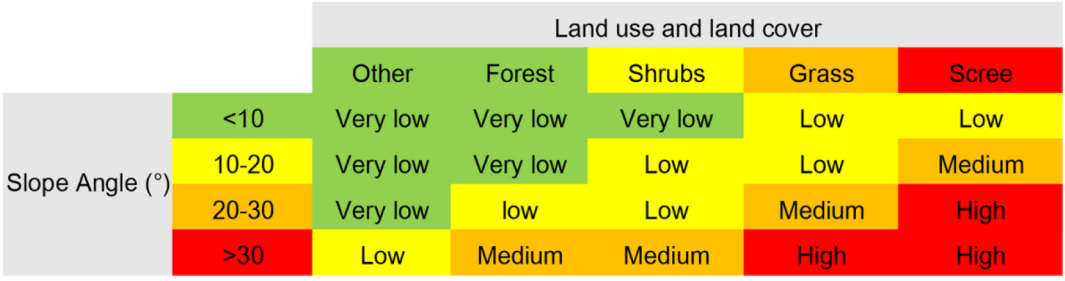
Land use and land cover
Other
Forest
Shrubs
Grass
Scree
Slope Angle (°)
<10
Very low
Very low
Very low
Low
Low
10-20
Very low
Very low
Low
Low
Medium
20-30
Very low
low
Low
Medium
High
>30
Low
Medium
Medium
High
High

Figure 8

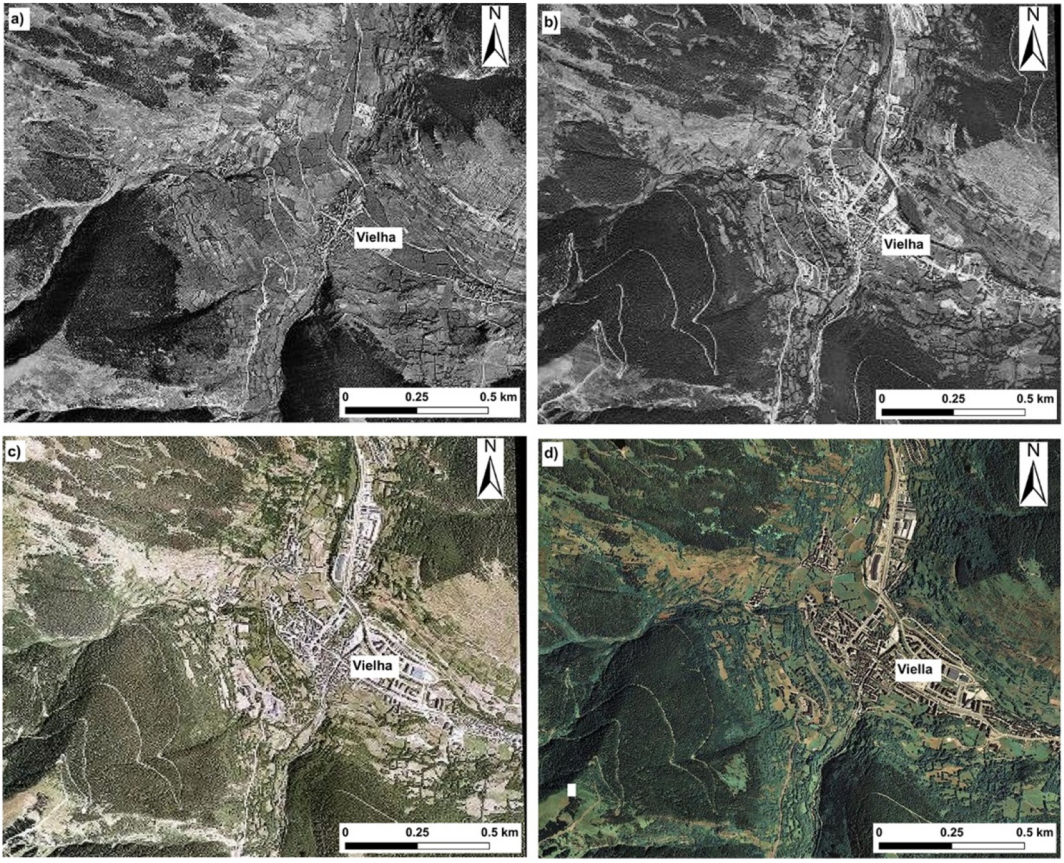
a)
N
Vielha
0
0.25
0.5 km
b)
N
Vielha
0
0.25
0.5 km
c)
N
Vielha
0
0.25
0.5 km
d)
N
Viella
0
0.25
0.5 km

Figure 9

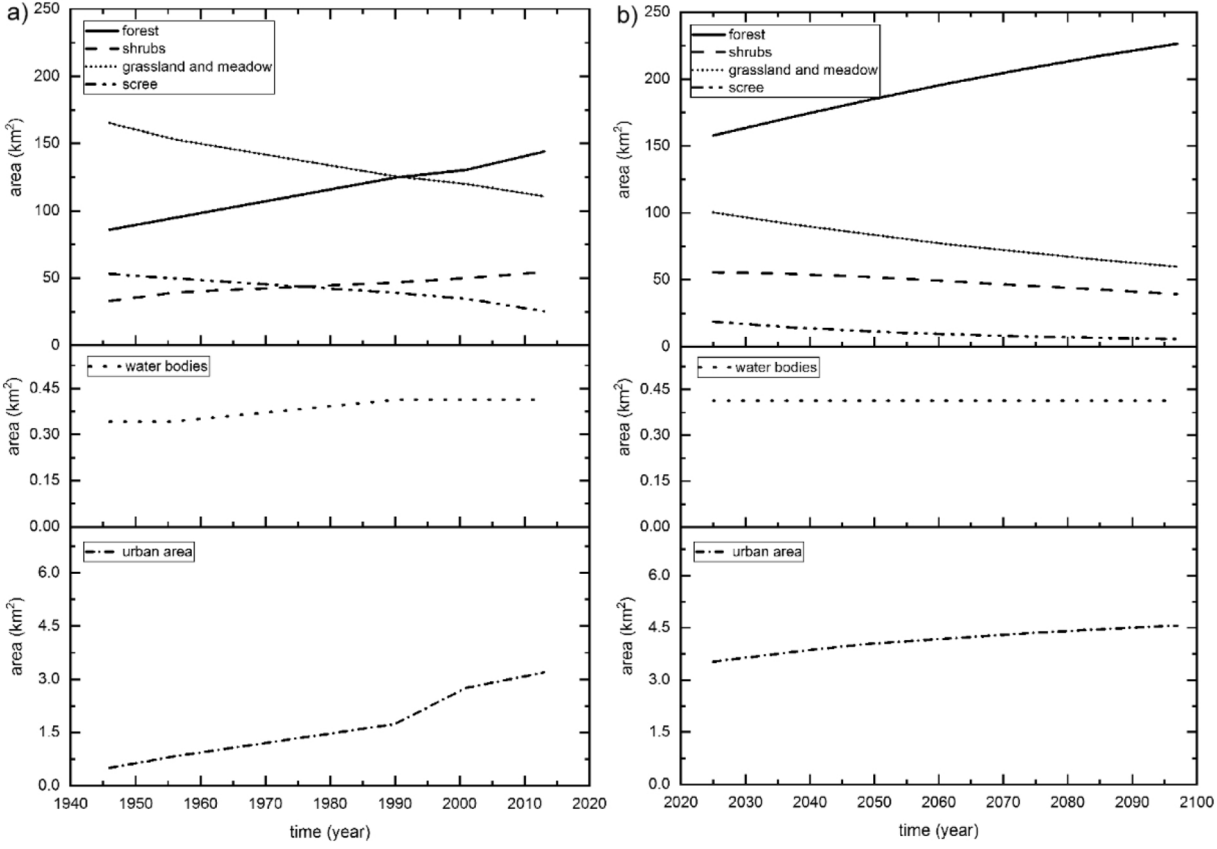
a)
b)
forest
shrubs
grassland and meadow
scree
water bodies
urban area
area (km²)
time (year)
1940
1950
1960
1970
1980
1990
2000
2010
2020
2030
2040
2050
2060
2070
2080
2090
2100

Figure 10

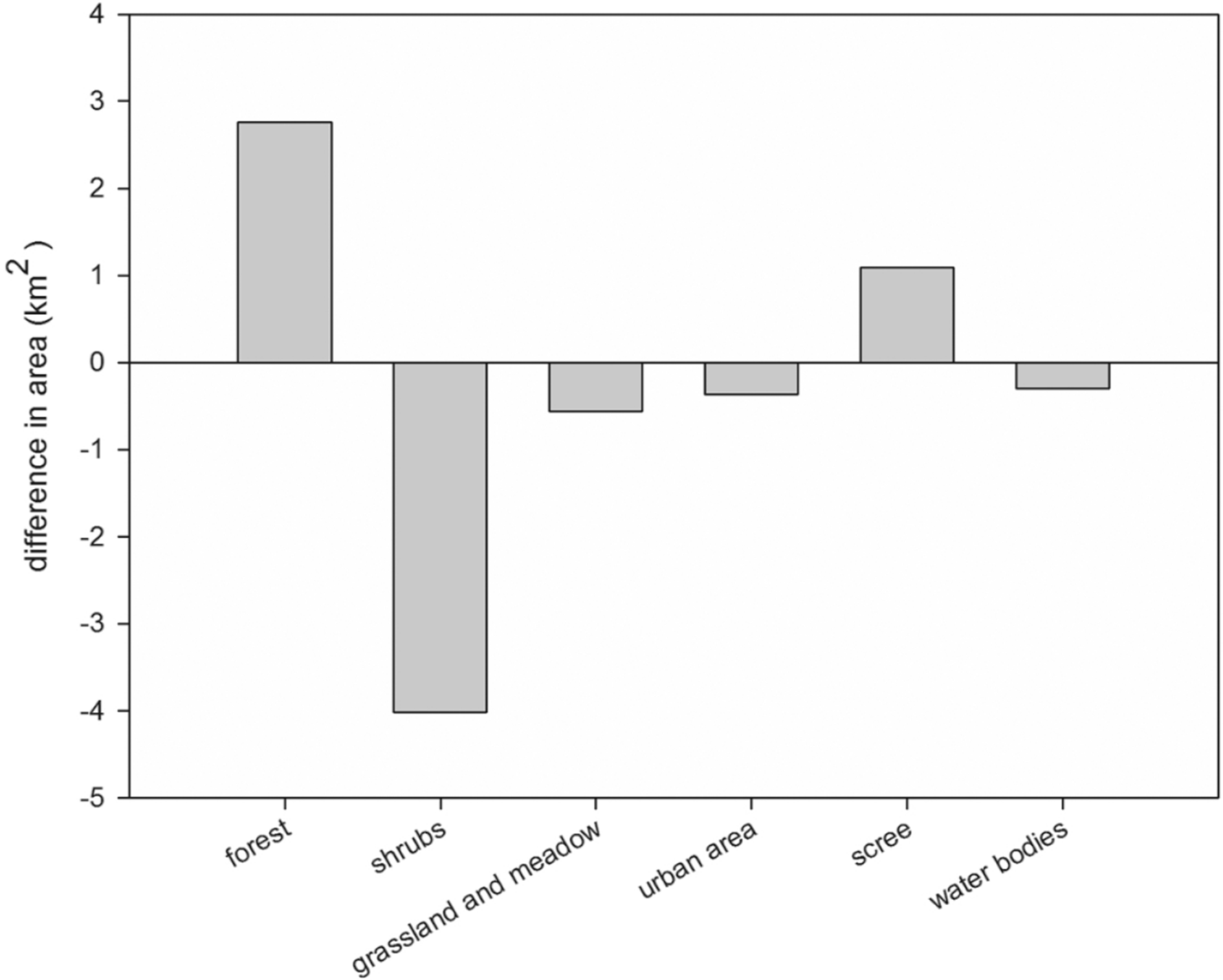
4
3
2
1
0
-1
-2
-3
-4
-5
difference in area (km2)
forest
shrubs
grassland and meadow
urban area
scree
water bodies

Figure 11

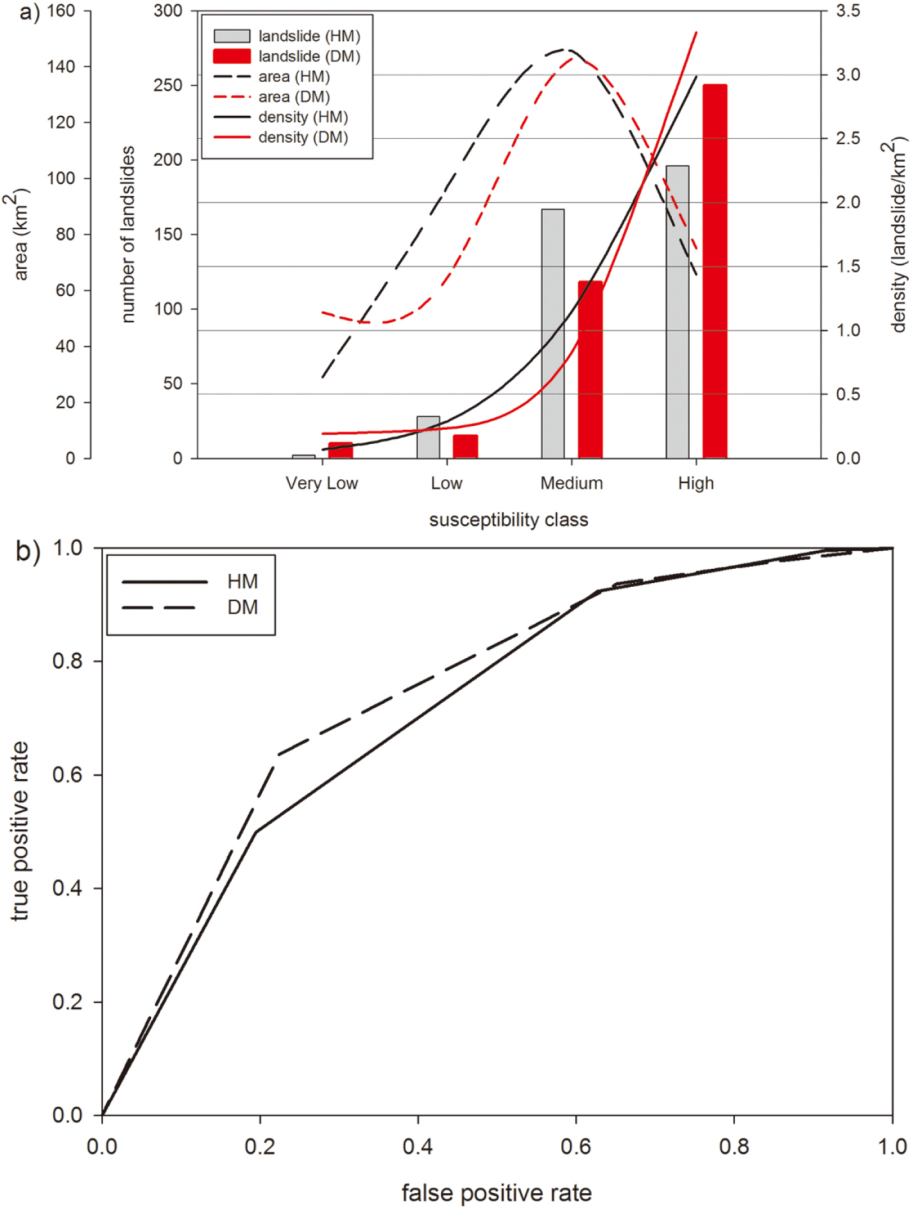
a)
landslide (HM)
landslide (DM)
area (HM)
area (DM)
density (HM)
density (DM)
area (km2)
number of landslides
density (landslide/km2)
Very Low
Low
Medium
High
susceptibility class
b)
HM
DM
true positive rate
false positive rate

Figure 12

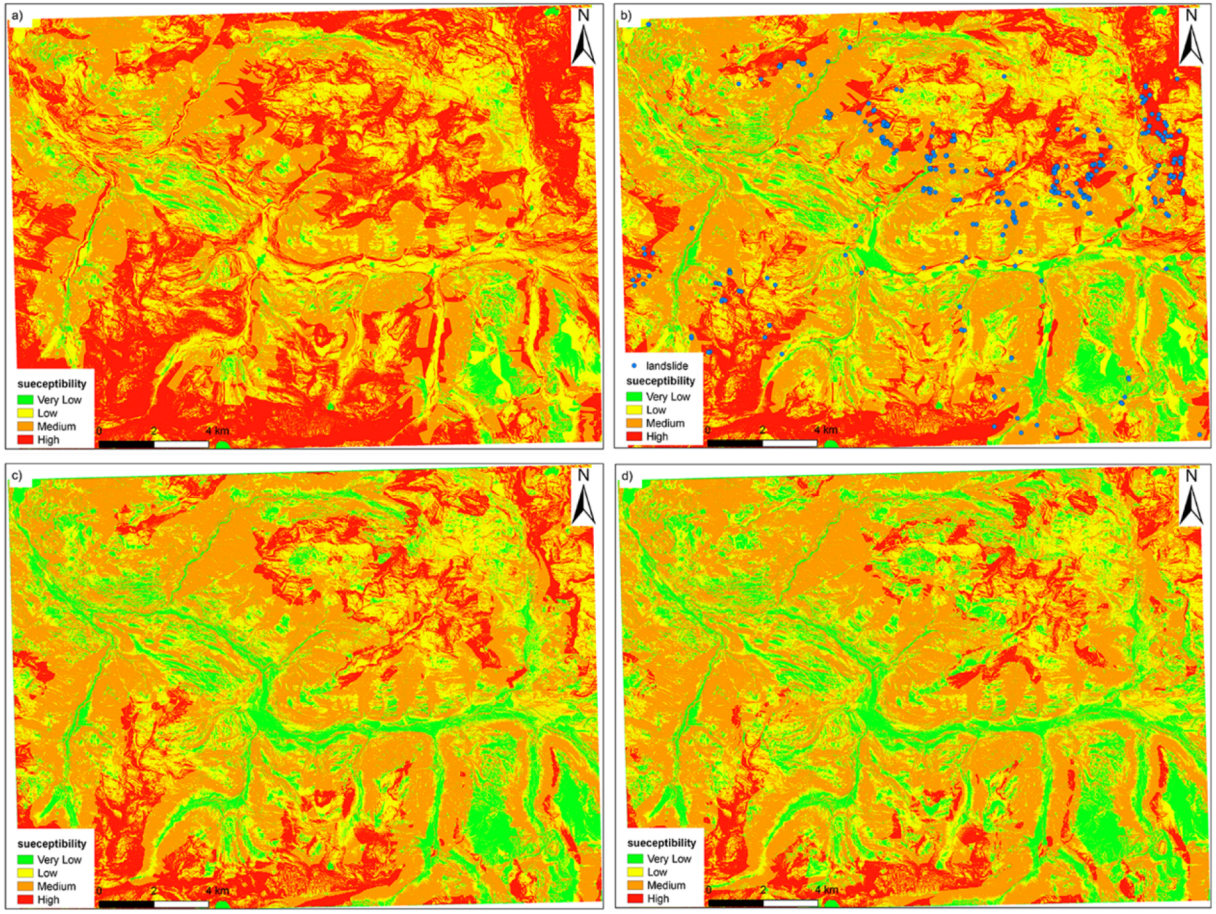
a)
N
sueceptibility
Very Low
Low
Medium
High
0
2
4 km
b)
N
landslide
sueceptibility
Very Low
Low
Medium
High
0
2
4 km
c)
N
sueceptibility
Very Low
Low
Medium
High
0
2
4 km
d)
N
sueceptibility
Very Low
Low
Medium
High
0
2
4 km

Figure 13

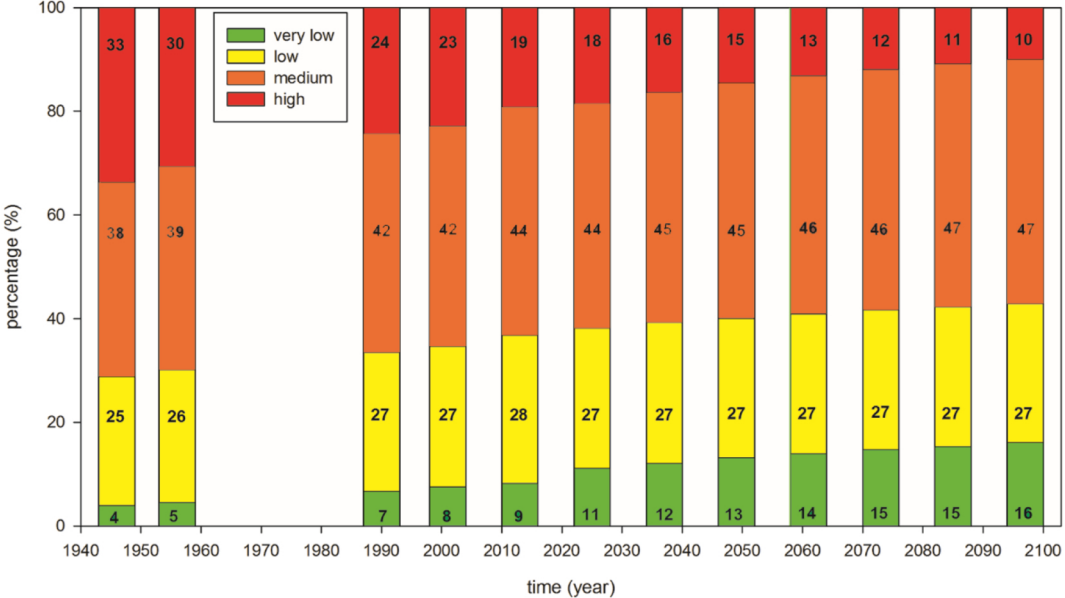
very low
low
medium
high
percentage (%)
time (year)
0
20
40
60
80
100
1940
1950
1960
1970
1980
1990
2000
2010
2020
2030
2040
2050
2060
2070
2080
2090
2100
33
30
24
23
19
18
16
15
13
12
11
10
38
39
42
42
44
44
45
45
46
46
47
47
25
26
27
27
28
27
27
27
27
27
27
27
4
5
7
8
9
11
12
13
14
15
15
16

Figure 14